Korean J. Chem. Eng., 36(3), 489-499 (2019)
DOI: 10.1007/s11814-018-0216-4

pISSN: 0256-1115
eISSN: 1975-7220

New insights into mechanistic aspects and structure of polycrystalline Cu/Cr/Ni metal oxide nanoclusters synthesized using *Eryngium campestre* and *Froriepia subpinnata*

Zahra Vaseghi*, Omid Tavakoli*,†, and Ali Nematollahzadeh,†**

*School of Chemical Engineering, College of Engineering, University of Tehran, Tehran 14176, Iran
**Chemical Engineering Department, University of Mohaghegh Ardabili, P. O. Box 179, Ardabil, Iran
(*Received 18 October 2018 • accepted 18 December 2018*)

Abstract−Novel nanoclusters (NCs) of Cu/Cr/Ni/O were produced by a green synthesis approach using leaf extracts of *E. campestre* and *F. subpinnata* at room temperature and pH 7. Characterization of the produced NCs using EDS, XRD, and FESEM revealed that *E. campestre* results in CuO-Cr_2O_3-NiO nanocomposites with average crystallite size of 29.2 nm, while binary and ternary Cu-Cr-Ni-O nanoalloys of averaged 9.8 nm crystallite size are produced using *F. subpinnata* leaf extract. In addition, bioreduction mechanism of the metal ions was investigated for both plant extracts by evaluating total phenolics/total flavonoids, HPLC chromatograms of the leaf extracts, and FTIR spectra of the extracts before and after the bioreduction reaction. It was found that phenolic acids are the main responsibility for the bioreduction of the metal ions. In particular, chlorogenic acid, rosmarinic acid, and syringic acids for the nanoalloys produced by reducing potential of *F. subpinnata*, and rosmarinic acid for the nanocomposites synthesized using *E. campestre* were identified as the main reducing agents. FTIR studies revealed that in CuO-Cr_2O_3-NiO nanocomposites, aliphatic and aldehyde amine groups and in Cu-Cr-Ni-O nanoalloys, aliphatic and aldehyde amine, and nitrile groups act as both capping and stabilizing ligands.

Keywords: Nanoalloy, Nanocomposite, Mechanism of Bioreduction, Plant Leaf Extract, Morphology

INTRODUCTION

Nanotechnology has revolutionized the world from different industries to medical science. In this respect, nanoparticles (NPs) and nanoclusters (NCs) are of particular importance due to their widespread applications [1]. Beside mono-metallic NPs, the production of binary and ternary nanocomposites/nanoalloys has developed because of their improved physical and chemical properties leading to their potential applications in catalyzed reactions [2-4], solar cells [5], gene delivery systems [6-8], and so on. Currently, a number of approaches are being used for the synthesis of multi-metallic NCs. In fact, the physical properties and application field of the produced NPs are heavily dependent upon their methods of preparation (*i.e.*, co-precipitation [9,10], reverse micelles [11,12], sol-gel [13,14], gel growth [15-18], and solvothermal technique [19,20]).

Production of metal/metal oxide NPs through bioreduction of metal ions compared to other methods of NP generation is more efficient and thus versatile [21]. On the other hand, from the green chemistry perspective, production of materials should not cause a threat to human health or the environment [22,23]. In this respect, the ingredients (*i.e.*, solvent, reducing agent, and capping/stabilizing agents) ought to be non-toxic and environmentally benign to be adapted to the green chemistry approach [1]. Although green synthesis of NPs is greatly developed in case of mono metallic NPs, less work is devoted to this issue for multi-metallic materials. For example, Rao and coworkers [24] have synthesized Ag-Au-Pd using the mixed extract of *Aegle marmelos* (leaf) and *Syzygium aromaticum* (bud). They have found that by varying the compositions of phytochemicals, different compositions of Ag-Au-Pd can be produced at ambient temperature. In another research, Zhan et al. [25] have developed a green synthesis method for simultaneous bioreduction of Au(III), Pd(II) precursor salts leading to the formation of Au-Pd bimetallic NPs. Degraded Pueraria starch (DPS) was utilized as both reducing and capping agents in the synthesis of Au/Ag bimetallic NPs by Xia et al. [26].

Using plant extracts as bioreducing and capping agent, the main challenge is to identify the mechanisms through which metal/metal oxide NPs are produced. Due to complexity of phytochemicals and abundance of the functional groups present in plant extracts, the feasibility of proposing the exact reaction mechanism may not be ascertained [27]. Phytochemical components responsible for bioreduction of metal ions and stabilizing the produced NCs are known as polyphenols (flavonoids, phenolic acids, and terpenoids), organic acids, and proteins [1]. There is also the probability of co-participation of some phytochemicals in the bioreduction of metal ions [28]. However, investigating Fourier transform infrared spectroscopy (FTIR) of both plant extracts and the produced NPs as well as high performance liquid chromatography (HPLC) of the extract could give rise to better understanding the functional groups and chemical compounds in the plant which may participate in the bioreduction process of precursor salts. Kesharwani et al. [29] proposed that quinones and plastohydroquinone molecules present in the plant leaf extract are responsible for the reduction of metal ions.

†To whom correspondence should be addressed.
E-mail: otavakoli@ut.ac.ir, nematollahzadeha@uma.ac.ir

Kasthuri et al. [30] used different concentrations of phyllanthin from *Phyllanthus amarus* to synthesize gold and silver NPs. FTIR analysis revealed that a shift of methoxy (-OCH_3) band after NP synthesis had occurred, which was attributed to the binding of -OCH_3 to NPs.

In our previous work, process parameters for maximizing trimetallic oxide Cu/Cr/Ni NP production using leaf extracts of *Eryngium campestre* and *Froriepia subpinnata* were optimized. Also, the produced NCs showed proper antibacterial activities against two pathogenic bacteria, namely *Escherichia coli* and *S. aureus* [31]. The main emphasis of the present study is on analyzing various hypothetical bioreduction mechanisms using different approaches. The NCs produced using the two leaf extracts at neutral pH were characterized using XRD, EDS, and FESEM analyses so that crystalline structure, elemental compositions, and morphologies were compared and discussed in detail.

EXPERIMENTAL PART

1. Chemicals

Metal salts including $CuSO_4{\cdot}5H_2O$, $Ni(NO_3)_2{\cdot}6H_2O$, and $Cr(NO_3)_3{\cdot}9H_2O$ were purchased from Merck, Germany. Sodium hydroxide and hydrochloric acid (37%) were supplied by Sigma-Aldrich. *Eryngium campestre* and *Froriepia subpinnata* were collected from north of Iran (Babol city). HPLC gradient grade methanol was purchased from Chem-lab NV (Belgium). Double distilled water was used throughout experiments for solution making and other purposes.

2. Plant Leaf Extracts and NC Green Synthesis

The procedure for preparing leaf extract was similar for the two plants. First, fresh leaves of *E. campestre* and *F. subpinnata* were collected, then separately rinsed with tap water and were washed twice with double-distilled water to remove contaminants and dust. Afterwards, the leaves were dried in shade for seven days. The dried leaves were uniformly powdered with household mill. By adding 5 g of each plant's leaf powder into 100 mL distilled water, leaf extracts were prepared. The resulting mixtures were then sonicated for 20 minutes at 400 W before being filtered with Whatman no. 1 filter paper. The obtained filtrate was used as plant extract for green synthesis of Cu/Cr/Ni metal oxide NCs [32].

In the green synthesis procedure, first, 0.01 M solution of the three metal precursor salts namely $CuSO_4{\cdot}5H_2O$, $Ni(NO_3)_2{\cdot}6H_2O$, and $Cr(NO_3)_3{\cdot}9H_2O$, was prepared in a 250 mL Erlenmeyer flask. *E. campestre* and *F. subpinnata* leaf extracts with the respective volume ratios of 2.4 and 1.0 were added into the mixed metal salts solution. By dropwise addition of sodium hydroxide solution (0.1 M) the pH of the reaction mixture was adjusted at 7.0. The bioreduction process for the synthesis of Cu/Cr/Ni ternary oxide NCs was completed within 10 minutes at room temperature. The produced NCs were separated from the solution by centrifugation at 20,000 rpm followed by successive washing with distilled water. The obtained wet powder was kept in a vacuum oven at 45 °C until being characterized.

3. Instrumentation and Apparatus

Morphological study of NCs was performed by field emission scanning electron microscopy (FESEM, MIRA3TESCAN-XMU). Crystalline structure of NCs was analyzed using X-ray diffractometer instrument with Cu Kα radiation using the Philips powder diffractometer system (λ=1.54060 nm, 40 Kv and 30 mA) in the range of 10-80° with 2°/min scanning rate. Ternary oxide Cu/Cr/Ni NCs composition was analyzed using energy dispersive X-ray spectroscopy (EDS), while the functional groups involved in bioreduction of metal salts were analyzed using Fourier transform infrared spectroscopy (FTIR spectroscopy RXI, Perkin Elmer, USA). The presence of potent antioxidants in the leaf extracts of *E. campestre* and *F. subpinnata* was investigated using high performance liquid chromatography (HPLC, Knauer, Eurospher I, 5 µm, 250× 4.6 mm, 100 °A).

4. Evaluation of Bioreduction Mechanism

Bioreduction mechanism could be investigated if the phytochemicals in the plant leaf extracts. which are supposed to take part in the bioreduction of metal ions and stabilizing/capping the resulting NCs. are identified. In this respect, efforts have been made to quantitatively specify the important bioactive compounds in *E. campestre* and *F. subpinnata* by determining total phenol and total flavonoid contents before and after the bioreduction reaction. In a similar approach, FTIR spectra of the plant extracts before and after the bioreduction process together with FTIR spectra of the produced Cu/Cr/Ni metal oxide NCs with plant capping were thoroughly investigated and compared with each other. In addition, HPLC chromatograms of the two plant extracts were evaluated.

4-1. Total Phenolic and Total Flavonoid Studies

Total phenolics of *E. campestre* and *F. subpinnata* was determined according to the method described by Singleton et al. [33] using the Folin-Ciocalteu assay. In a typical procedure, an aliquot (1 mL) of the extracts or standard solution of gallic acid (20, 40, 60, 80, and 100 mg/L) was added into a flask containing 9 mL deionized water. Afterwards, 1 mL of Folin-Ciocalteu phenol reagent was added to the mixture followed by shaking at 150 rpm at an orbital shaker. After 5 min, 10 mL of Na_2CO_3 solution (7%) was added to the mixture. Using deionized water the solution was diluted up to the volume of 25 mL and was maintained for 90 min at room temperature. UV-Vis absorbance of the resulting solution against the blank was evaluated at 750 nm using UV-Vis spectrophotometer (Nanolytik® NanoSpec 2 spectrophotometer). Amount of total phenolics in the extracts was measured according to mg gallic acid equivalents (GAE)/1 g dry weight. The method developed by Zhishen et al. [34] was utilized to estimate total flavonoid content of *E. campestre* and *F. subpinnata* extracts using aluminum chloride calorimetric assay. An aliquot (1 mL) of the extracts or standard solution of catechin (20, 40, 60, 80, and 100 mL) was added to a 25 mL volumetric flask containing 4 mL deionized water followed by the addition of 0.3 mL of Na_2CO_3 (5%) solution. After 5 minutes, 0.3 mL of $AlCl_3$ (10%) was added to the mixture. One minute later, 2 mL of NaOH (1 M) solution was added and the total volume was adjusted to 10 mL using deionized water. The solution was mixed completely before detecting its absorbance against reagent blank at 510 nm. Total flavonoid content of the extracts was measured according to mg catechin equivalents (CE)/1 g dry weight. Both assays were triplicated and the mean values were reported.

4-2. FTIR Studies

FTIR spectra were recorded in solid and liquid phases using KBr

aperture plate technique in the range of 400-4,000 cm^{-1}. In a typical procedure, FTIR analysis was performed on the aqueous leaf extracts of *E. campestre* and *F. subpinnata*. After completion of the bioreduction process resulting from the addition of the leaf extracts with defined volume ratio (2.5 for *E. campestre* and 1 for *F. subpinnata*) to 0.01 M solution of precursor metal salts ($CuSO_4 \cdot 5H_2O$, $Ni(NO_3)_2 \cdot 6H_2O$, and $Cr(NO_3)_3 \cdot 9H_2O$), the produced NCs were separated by centrifugation, and the supernatants (exhausted plant extracts) were characterized by FTIR analysis. Comparing FTIR peaks of the exhausted plant extracts with those of pure plant extracts could give rise to chemical identification of the functional groups of the plants most probably involved in the reduction of metal salts and capping/stabilizing of the NCs.

4-3. HPLC Studies

HPLC analysis was performed to better elucidate the types of phenolic acids present in the plant phytochemicals which may have been involved in the bioreduction process. A Knauer HPLC system including stainless steel column (250 mm×4.6 mm) was used in the entire analysis. A mixture of trifluoroacetic acid (TFA) with water and methanol with a flow rate of 1.0 mL/min was used as the mobile phase. Twelve phenolic acids including caffeic acid, chlorogenic acid, syringic acid, rosmarinic acid, 3,4-dihydroxy benzoic acid, gallic acid, vanillic acid, salicylic acid, 2,5-dihydroxybenzoic acid, para coumaric acid, ferulic acid, and cinnamic acid were used as standards.

RESULTS AND DISCUSSION

1. Characterization of NCs

1-1. Composition and Crystallinity

Composition of NCs synthesized using *E. campestre* (EC-NCs) and *F. subpinnata* (FS-NCs) leaf extracts was analyzed using EDS

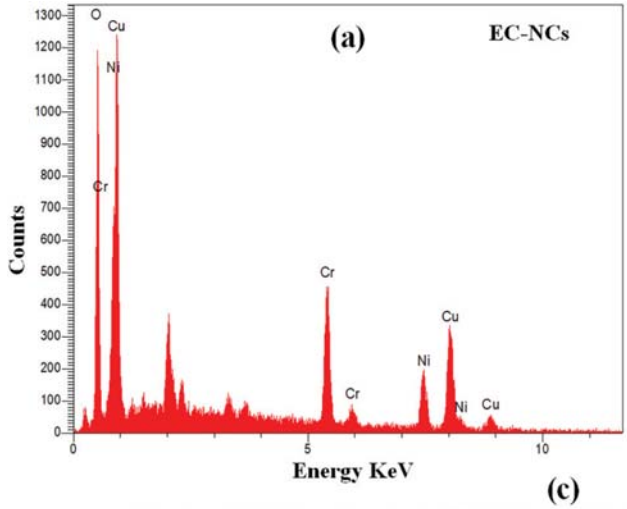

(b)

Element	W%	A%	Error
O	28.42	59.70	3.5695
Cr	15.02	9.71	0.6201
Ni	15.65	8.96	0.8740
Cu	40.91	21.64	0.8740
Total	100.00	100.00	-

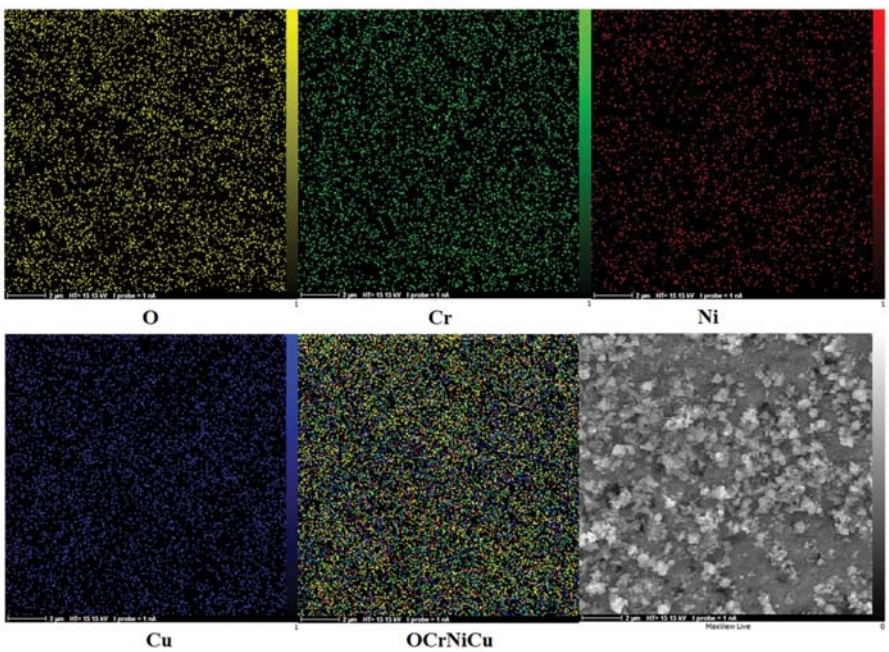

Fig. 1. (a) EDS spectroscopy, (b) atomic and weight compositions and (c) selected area elemental mapping of Cu/Cr/Ni oxide NCs synthesized using *E. campestre*.

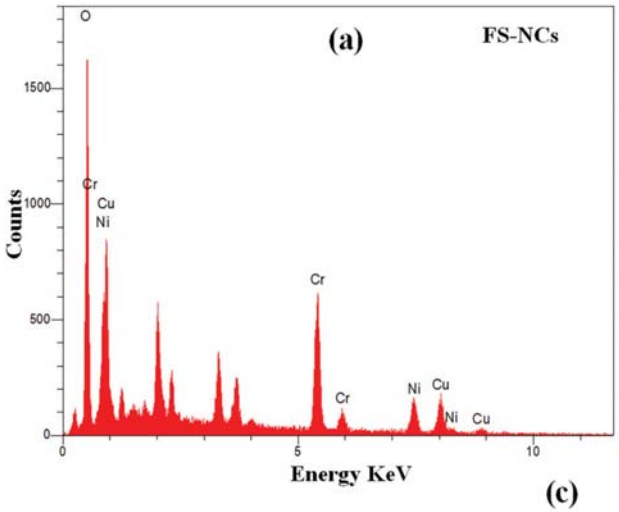

(b)

Element	W%	A%	Error
O	40.03	70.48	8.5416
Cr	24.41	13.22	0.9810
Ni	14.65	7.03	0.7329
Cu	20.91	9.27	0.7329
Total	100.00	100.00	-

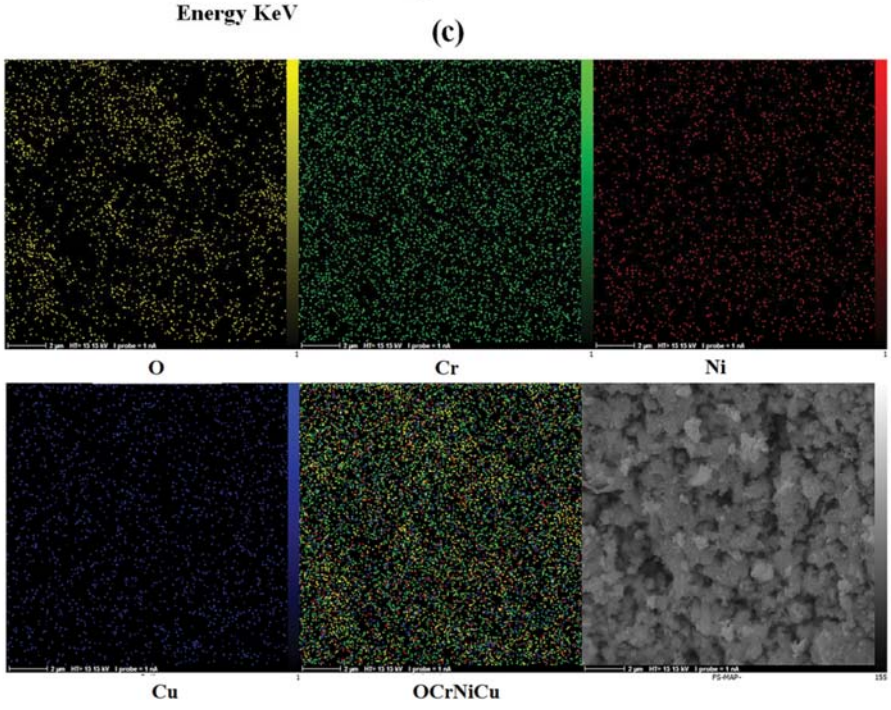

Fig. 2. (a) EDS spectroscopy, (b) atomic and weight compositions and (c) selected area elemental mapping of Cu/Cr/Ni oxide NCs synthesized using *F. subpinnata*.

spectroscopy to certify the presence of elemental copper, chromium, and nickel in the two types of the nano-powders (Fig. 1 and Fig. 2). It can be seen that strong signals at ~1, 5.5, 7.5, and 0.5 KeV are approximately the region for copper, chromium, nickel, and oxygen in EC-NCs and FS-NCs, respectively [35-37]. However, composition of the elements was different for the two types of the nano-powders (Fig. 1(b) and Fig. 2(b)). More oxygen atoms involved in the chemical composition of FS-NCs, while nickel composition remained almost unchanged and compositions of copper and chromium varied completely. EC-NCs were rich in metallic copper; whereas more balanced distribution of composition was evident in FS-NCs. Selected area elemental mappings of EC-NCs and FS-NCs are presented in Fig. 1(c) and Fig. 2(c). In these figures, oxygen, chromium, nickel, and copper are, respectively, represented by yellow, green, red, and blue colors. Also, a frame containing all of the mentioned elements is presented. Although assumption of definite configurations of NCs from these images is not feasible, mixed configuration of elements is more evident for FS-NCs. On the other hand, elemental mapping of EC-NCs exhibits the existence of similar colors which are representative of identical elements with atomic oxygen in their vicinity.

To confirm the formation of copper, chromium, nickel oxides and other probable compounds which may have been formed in the green bioreduction process by the two plant extracts, the obtained powder was characterized by XRD. Fig. 3 shows that the in EC-NCs and FS-NCs are almost the same. However, phase analysis by X'Pert highscore plus software (version 2.2) revealed that the most intense peaks for XRD pattern of EC-NCs at 36.73°, 43.48°, 63.14°, and 75.33° are mainly attributed to the chemical structures of individual metal oxides such as nickel oxide (NiO), copper oxide (CuO), and chromium oxide. The predicted location of these structures and the corresponding crystallite size calculated using Scherer solver

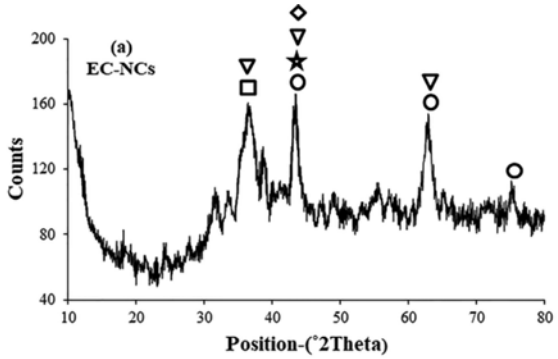

Nickel Oxide (NiO)	Rhombohedral	Crystallite size: 161 A	○
Copper Oxide (CuO)	Monoclinic	Crystallite size: 310 A	□
Chromium Oxide (Cr_2O_3)	Cubic	Crystallite size: 404 A	▽
Copper (Cu)	Cubic	-	★
Chromium (Cr)	Cubic	-	◇

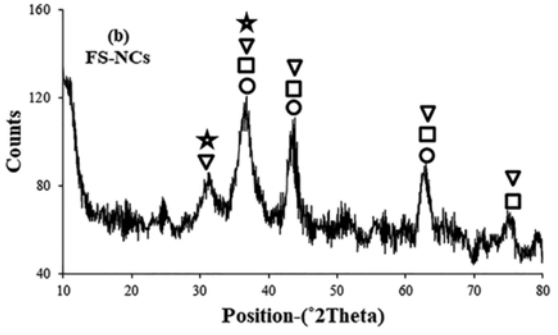

Nickel Copper Chromium Oxide ($Ni_{0.8}Cu_{0.2}Cr_2O_4$)	Tetragonal	Crystallite size: 96 A	○
Nickel Copper Oxide ($Ni_{0.95}Cu_{0.05}O$)	Cubic	Crystallite size: 99 A	□
Copper Chromium Oxide ($CuCrO_2$)	Rhombohedral	Crystallite size: 99 A	▽
Nickel Chromium Oxide ($NiCr_2O_4$)	Tetragonal	-	★

Fig. 3. XRD patterns of Cu/Cr/Ni metal oxide NCs obtained using (a) *E. campestre* leaf extract and (b) *F. subpinnata* leaf extract.

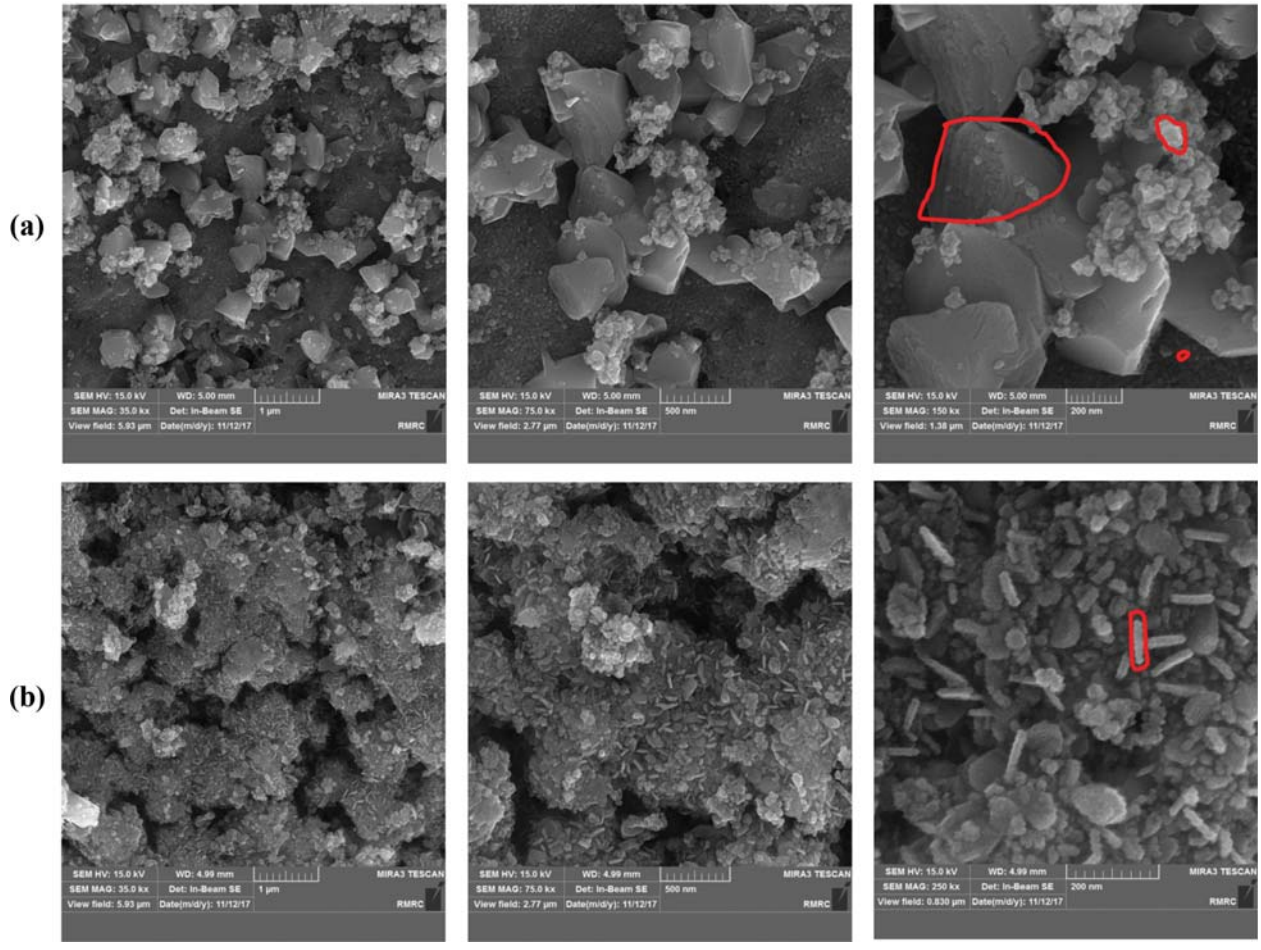

Fig. 4. FESEM images of Cu/Cr/Ni metal oxide NCs at different magnifications: (a) NCs from *E. campestre* and (b) NCs from *F. subpinnata*.

by the software are given in Fig. 3(a). As it was expected, significant difference was observed among the calculated crystallite sizes (16.1, 31.0, and 40.4 nm for the NiO, CuO, and Cr_2O_3 NPs). Interestingly, the structural prediction for FS-NCs at the angles of 31.33°, 36.68°, 43.48°, 62.77°, and 75.58° demonstrates different binary and ternary nanoalloys including nickel copper chromium oxide ($Ni_{0.8}Cu_{0.2}Cr_2O_4$), nickel copper oxide ($Ni_{0.95}Cu_{0.05}O$), copper chromium oxide ($CuCrO_2$), and nickel chromium oxide ($NiCr_2O_4$). Thus, both types of the produced nanomaterials have polycrystalline structure. In addition, crystallite size for these structures was almost identical and the calculated average size was 9.8 nm.

1-2. Size and Morphology

Size and morphology of the EC-NCs and FS-NCs were assessed using FESEM images. The images were presented at different magnifications (1 μm, 500 nm, and 200 nm) for the two types of nano-powders. As is apparent from these Figs, the morphologies of Cu/Cr/Ni nano-powders produced using the two leaf extracts are completely different. While three distinct structures with considerably varied morphologies are evident in the FESEM images of EC-NCs, FS-NCs possess almost uniform plate like shape. Two hypotheses may arise from flat plate-like clusters observed in Fig. 4(b). In the first hypothesis, the NPs may have aggregated during preparation process and thus stick together by physical interactions. The second theory is based on the existence of chemical binding among various NPs leading to the formation of binary and ternary nanoalloys out of copper, chromium, nickel, and oxygen. However, regarding the obtained results from XRD pattern, which evidenced the presence of binary and ternary nanostructures in FS-NCs, the second hypothesis is rejected. Thus, it may be inferred that bioreduction of the precursor salts ($CuSO_4$, $Cr(NO_3)_3$, and $Ni(NO_3)_2$ with *E. campestre* at neutral pH leads to the formation of individual metal/metal oxide copper, chromium, and nickel NPs (CuO-Cr_2O_3-NiO nanocomposites), whereas the use of *F. subpinnata* results in the synthesis of flat nano-plate shaped alloys out of the three metals (*i.e.* Cu-Cr-Ni-O nanoalloys).

Also, using imageJ software, the mean thickness of NCs was measured. However, due to existence of various morphologies in the EC-NCs, the thickness was calculated for each of the three shapes represented in Fig. 4(a). The calculated thickness values for the EC-NCs and FS-NCs are given in Table 1. Obtained results regarding NP sizes indicate that utilization of *E. campestre* and *F. subpinnata* leaf extracts resulted in a variety of crystallite sizes. In this way, by merely selecting the appropriate plant extract, controlling the size of produced NCs could be feasible. Furthermore, upon comparison with the crystallite sizes calculated using Scherrer equation from the XRD spectra, good agreement was evident for both types of nanomaterials (nanocomposites from *E. campestre* and nanoalloys from *F. subpinnata*).

Table 1. Average size (nm) of *E. campestre* and *F. subpinnata* mediated NCs particles or nanoalloys

E. campestre-mediated particles			*F. subpinnata*-mediated nanoalloy
Small	Medium	Large	
6.36	17.21	72.04	11.37

2. Mechanism of Bioreduction

A four-step process is suggested for the reduction of Cu^{2+}, Cr^{3+}, and Ni^{2+} ions by the aqueous leaf extracts of *E. campestre* and *F. subpinnata*. In an aqueous solution, the precursor salts of copper sulfate, nickel nitrate, and chromium nitrate are decomposed into the negatively charge anions of sulfate and nitrate and the positively charge Cu^{2+}, Cr^{3+}, and Ni^{2+}. The hydrated electrons from the aqueous leaf extracts of *E. campestre* and *F. subpinnata* convert the mentioned metal ions into zero-valent metals (Cu^0, Cr^0, and Ni^0) during nucleation process. In the next step, oxygen may bind to the metals either from the atmosphere or from the degrading phytochemicals available in the two leaf extract to produce metal oxides. Afterwards, a large number of nanozero-valent metals agglomerate so that Cu^0_n, Cr^0_n, Ni^0_n, or different combinations of these metals with each other and with molecular oxygen are formed during growth process. The metals are joined together since the binding energy between two metal atoms is much stronger than the binding energy between metal atom and the solvent as was previously reported by Pandian et al. [38]. Thus, copper, chromium, and nickel atoms attract each other by diffusion and grow as bulk materials during some coalescence processes. Finally, the phytochemicals in the two plant extracts stabilize the produced NPs by an organic cover surrounding them. Note that, as was confirmed by XRD and FESEM, different mono, binary, and ternary compounds may be formed as a result of bioreduction reaction by the two plant extracts.

For more detailed investigating the mechanism of Cu/Cr/Ni metal oxide NP synthesis, phytochemical characterization of the two plant extracts was required. For this purpose, total phenols and total flavonoids of *E. campestre* and *F. subpinnata* leaf extracts before and after bioreduction reaction was determined (Table 2).

Data presented in Table 2 clearly outlines that there is no significant difference between the total phenols and flavonoids of the two plant extracts before the reaction, although *F. subpinnata* showed slightly better results. After the reaction completed, total phenolics and total flavonoids contents decreased in both leaf extract. However, decline in total phenolics content was more significant than total flavonoid content. This indicates that phenolic compounds such as phenolic acids in *E. campestre* and *F. subpin-*

Table 2. Total phenolics and flavonoids content of *E. campestre* and *F. subpinnata* leaf extracts before and after bioreduction reaction

Plant extract	Total phenolics (mg GAE/1g-DW)		Total flavonoids (mg QUE/1g-DW)		$\frac{\text{Total flavonoids}}{\text{Total phenolics}}$	
	Before	After	Before	After	Before	After
E. campestre	61.7	40.9	30.6	24.6	0.50	0.60
F. subpinnata	73.6	57.8	34.4	27.3	0.47	0.47

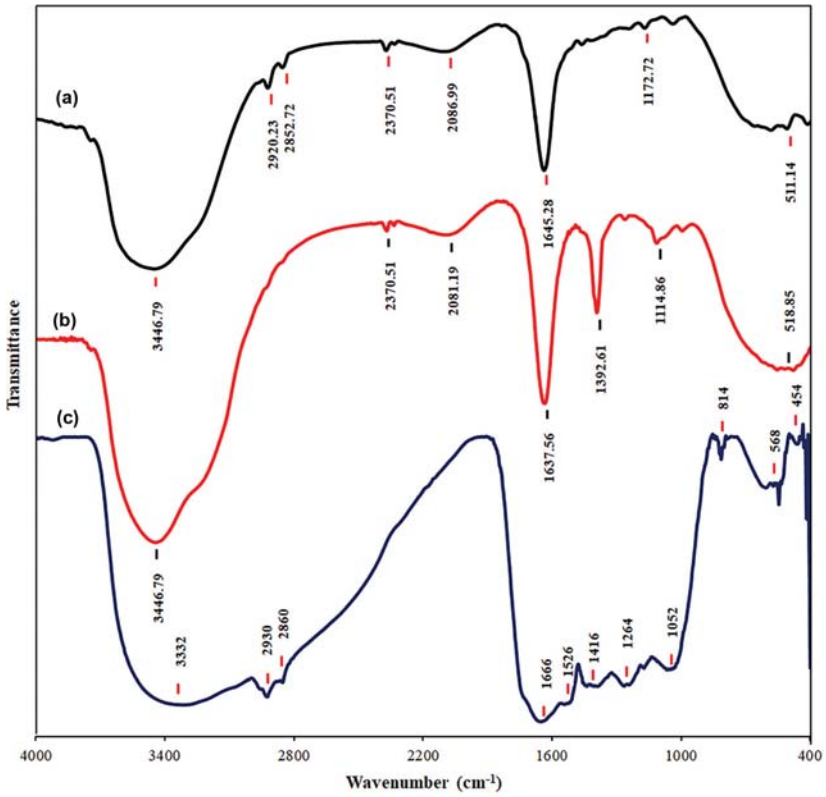

Fig. 5. FTIR spectrum of (a) *E. campestre* aqueous leaf extract before bioreduction process and (b) solution obtained by centrifugation after the bioreduction process and (c) EC-NCs with plant capping.

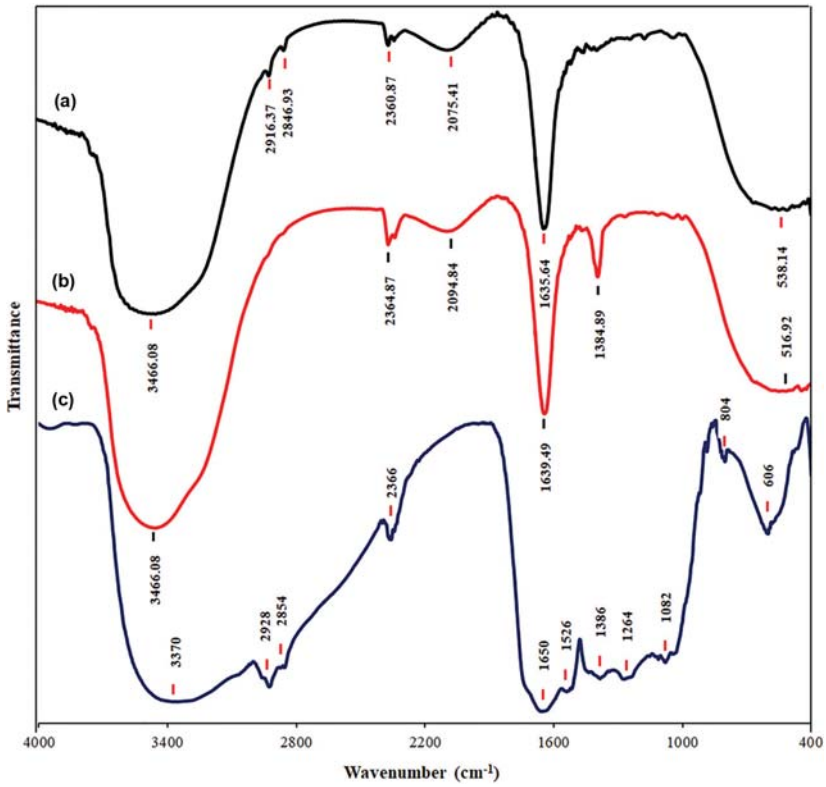

Fig. 6. FTIR spectrum of (a) *F. subpinnata* aqueous leaf extract before bioreduction process and (b) solution obtained by centrifugation after the bioreduction process and (c) FS-NCs with plant capping.

nata leaf extracts are more involved in the bioreduction reaction of copper, chromium, and nickel ions. More specifically, since total phenolic content of *E. campestre* showed more decline than that for *F. subpinnata* (33.7% versus 21.5%). it may be concluded that bioreduction of copper, chromium, and nickel ions and CuO-Cr_2O_3-NiO nanocomposite formation requires participation of greater amount of phytochemicals of *E. campestre* leaf extract. This may lead to the formation of new secondary metabolites. Chen et al. [39] also measured total flavonoids of alfalfa extract before the reaction and also after the completion of the reaction for Ni nanoparticle synthesis, and found that flavonoid content of the extract had tremendously decreases. This finding is consistent with our results concerning total flavonoids change during the course of bioreduction reaction for *E. campestre* and *F. subpinnata* extracts.

FTIR spectra of aqueous leaf extracts of *E. campestre* and *F. subpinnata* before and after the synthesis of NCs as well as the synthesized ternary NCs with plant capping are, respectively, depicted in Fig. 5(a)-(c) and Fig. 6(a)-(c). As is apparent from these Figs, the trend in FTIR spectra is almost the same for the two leaf extracts, which reinforces the possibility of similar phyto-constituents of the two leaf extracts being involved in the bioreduction process. In case of *E. campestre*, some intense peaks were observed at 3,446.79, 2,920.23 and 2,852.72, 2,370.51, 2,086.99, 1,645.28, 1,172.72, and 511 cm^{-1}. Almost similar peak locations were found for *F. subpinnata* aqueous leaf extract at 3,466.08, 2,916.37, 2,846.93, 2,360.87, 2,075.41, 1,635.64, and 538.14 cm^{-1} (Fig. 6(a)). This indicates that the functional groups in the two leaf extracts which take part in the bioreduction process and capping the produced NCs are in many aspects identical. In both leaf extracts, the wide and strong peak observed at 3,466 cm^{-1} corresponds to O-H groups present in alcohols and phenols as well as N-H stretching of hydrogen bonded amine groups [40,41].

Bioreducing potential of phenolic compounds has been proven in several researches [36,42,43]. It is agreed that a direct relationship exists between antioxidant activity of the plant extracts and the number of phenolic groups. So, free radical scavenging potential of the plant extract, which is created as a result of efficient delocalization of the unpaired electrons, is provided by large number of phenolic groups [44]. Furthermore, the peaks at 2,920.23 cm^{-1} and 2,852.72 cm^{-1} are assigned to aliphatic C-H stretching and also C-H of aldehyde amine groups [45-47]. Also, the peak at 2,370.51 cm^{-1} is assigned to C≡N of nitriles, while the noticeable intense peak at 1,645.28 cm^{-1} corresponds to -OH bending mode or C=O stretching vibration of carbonyl and carboxylic group of amide I [46,48]. The peak at 1,172.72 cm^{-1} is attributed to C-O stretching vibrations of polyols including flavones, polysaccharides and reducing sugars in the plant extract [49]. Finally, the location of peak at 511.14 cm^{-1} represents C-H of alkynes [50].

On the other hand, it is clear from Figs. 5 and 6 that the FTIR spectra of the two plant extracts before and after the bioreduction are changed in some locations. Comparing the changes in the peak locations of plant extracts (Fig. 5(a), (b)) and Fig. 6(a), (b)) with FTIR spectra of the capped NCs (Fig. 5(c) and Fig. 6(c)), appropriate speculation can be made regarding the involved reducing and capping agents. As is evident from these figures, the peaks at around 2,920 and 2,950 cm^{-1} have disappeared in the extracts after

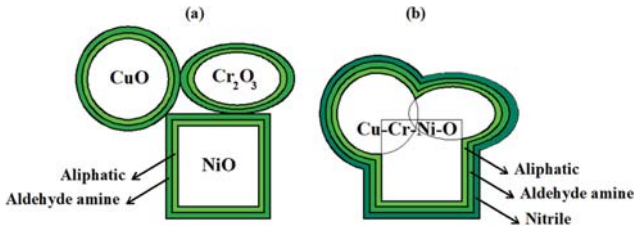

Fig. 7. Schematic representation of capping ligands from (a) *E. campestre* surrounding CuO-Cr_2O_3-NiO nanocomposites and (b) *F. subpinnata* surrounding Cu-Cr-Ni-O nanoalloys.

bioreduction process, while they are depicted with slight change in wavenumber in the produced NCs (around 2,930 and 2,960 cm^{-1}). This implies that aliphatic and also aldehyde amine groups of *E. campestre* and *F. subpinnata* aqueous leaf extracts may act as capping ligands in the synthesizes of NCs, thereby stabilizing the produced NCs. Also, the peak at 2,370.51 cm^{-1} has completely disappeared in the FTIR spectrum of EC-NCs (Fig. 7(c)), whereas in the FTIR spectrum of FS-NCs, the peak at around 2,366 cm^{-1} still exists, leading to the hypothesis that C≡N of nitriles acts both as reducing and capping agent in *F. subpinnata*, while only participates in the bioreduction process in *E. campestre*. Moreover, new peaks at 1,392.61 and 1,384.89 cm^{-1} are evident in the FTIR spectra of *E. campestre* and *F. subpinnata* extracts after the bioreduction process, which are mainly assigned to C-C bond of aromatic

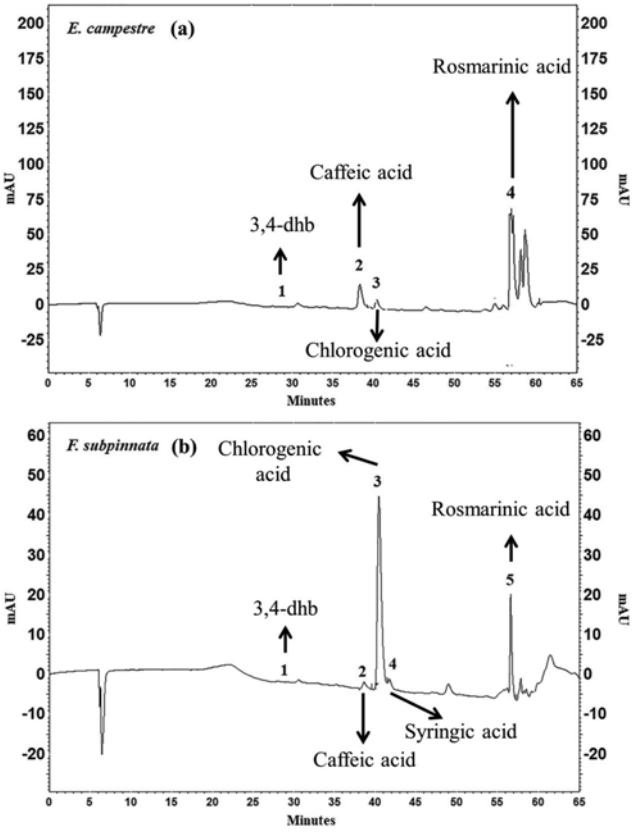

Fig. 8. HPLC chromatogram of (a) *E. campestre* leaf extract and (b) *F. subpinnata* leaf extract.

ring or amide II group [50], as new biologically active compounds may have been produced as a result of precursor metal salts reduction by the plant extracts. Probable capping ligands from *E. campestre* and *F. subpinnata*, respectively, covering CuO-Cr_2O_3-NiO nanocomposites and Cu-Cr-Ni-O nanoalloys are depicted in Fig. 7.

HPLC analysis of *E. campestre* and *F. subpinnata* leaf extracts revealed the presence of some phenolic acids out of the twelve standard phenolic acids as potent antioxidants. Existence of (1) 3,4-dihydroxy benzoic acid (3,4-dhb), (2) caffeic acid, (3) chlorogenic acid, (4) and rosmarinic acid in *E. campestre* and (1) 3,4-dihydroxy benzoic acid, (2) caffeic acid, (3) chlorogenic acid, (4) syringic acid, and (5) rosmarinic acid in *F. subpinnata* leaf extracts was approved (Fig. 8). The quantitative investigation of the mentioned phenolic acids in the two leaf extracts as well as their corresponding relative standard deviation (RSD) is given in Table 3. While *E. campestre* leaf extract was rich in rosmarinic acid (13.55 mg/total extract), chlorogenic acid had the greatest quantity in *F. subpinnata* followed by rosmarinic acid and syringic acid (8.87,

Table 3. Identified phenolic acids in the HPLC chromatogram of *E. campestre* and *F. subpinnata* leaf extracts

Phenolic acids	Quantity (mg active compound/total extract)		RSD	
	E. campestre	*F. subpinnata*	*E. campestre*	*F. subpinnata*
Caffeic acid	3.46	1.34	0.01	0.05
Chlorogenic acid	1.19	8.87	0.00	0.02
Syringic acid	-	1.87	-	0.01
Rosmarinic acid	13.55	3.94	0.02	0.02
3,4-dhb	0.66	0.77	0.07	0.00

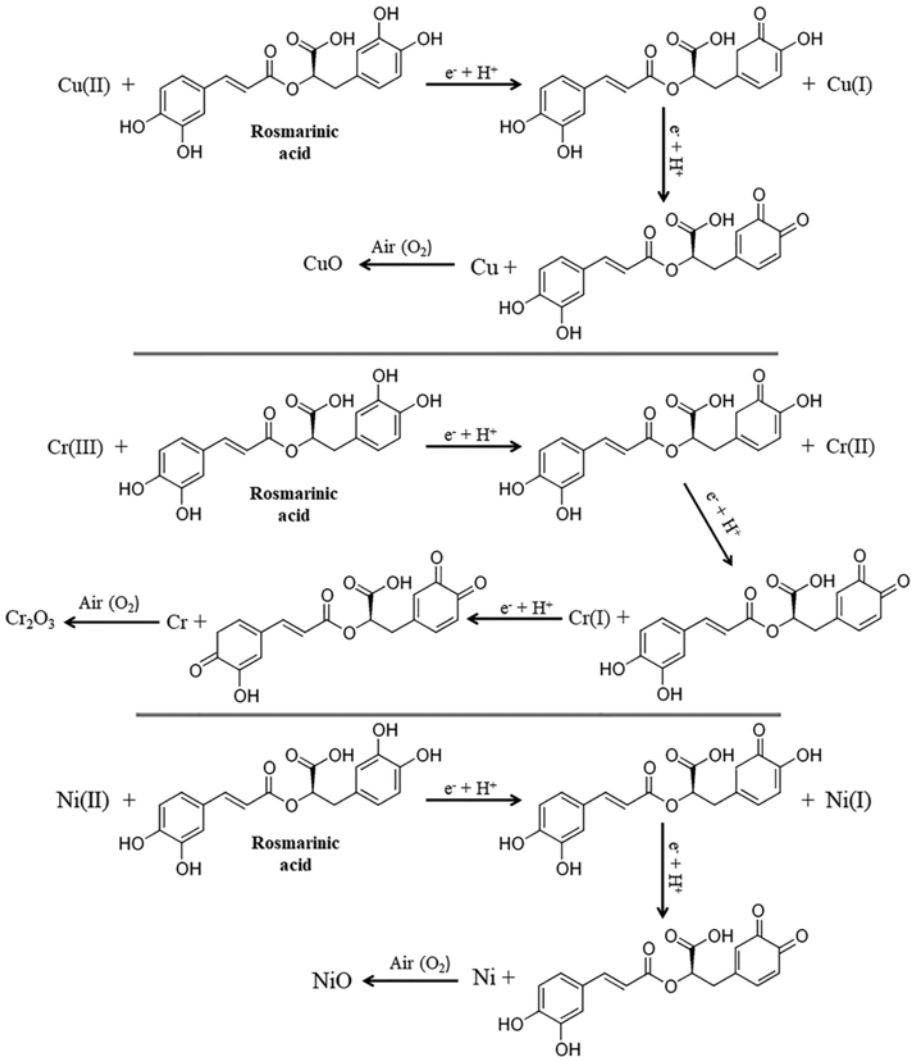

Fig. 9. Probable bioreduction mechanism for the synthesis of CuO/Cr_2O_3/NiO nanocomposites using the phytochemicals in *E. campestre* leaf extract.

3.94, and 1.87 mg/total extract, respectively). However, in case of *E. campestre* leaf extract, the presence of other phytochemicals such as kaempferol, rutin, quercetin besides the mentioned phenolic acids has been reported [51,52]. This indicates that other phytoconstituents may also have participated in bioreducing metal ions. Potential application of phenolic acids as green antioxidants lie in their ability to chelate different metal ions through ortho-phenolic groups [53]. Edison and Sethuraman [54] indicated that silver NPs have been synthesized due to formation of an intermediate complex of silver ions with the phenolic hydroxyl groups of gallic acid, which was consequently oxidized into quinone. Thus, it can be inferred that the released hydrogen atoms during oxidation of phenolic acids in the extracts of *E. campestre* and *F. subpinnata* can take part in bioreduction of Cu^{2+}, Cr^{3+}, and Ni^{2+} ions and subsequent synthesis of polystructured nanomaterials.

Due to the complex nature of phytochemicals present in the leaf extracts and involvement of three metal ions in the reaction mixture, prediction of exact mechanism for bioreduction reaction may not be feasible. However, based on the obtained results from total phenolics/total flavonoids assays, FTIR spectra of the extracts before and after reduction, and HPLC chromatograms of the two plant extracts, the presence of some phenolic acids which are the main responsibility for bioreduction reaction is evident in *E. campestre* and *F. subpinnata*. Thus, the mechanism of bioreduction has been given based on the reducing capability of those phenolic acids abundantly present in the extracts (rosmarinic acid in *E. campestre* and chlorogenic acid, rosmarinic acid, and syringic acid in *F. subpinnata*). In addition, as was discussed earlier in the manuscript, *E. campestre* and *F. subpinnata* leaf extracts showed different attitudes toward simultaneous reduction of Cu^{2+}, Cr^{3+}, and Ni^{2+} ions. Thus, in case of *E. campestre* leaf extract, nanocomposites of CuO-Cr_2O_3-NiO have been produced, while the use of *F. subpinnata* leaf extract has resulted in different binary or ternary nanoalloys of Cu-Cr-Ni-O. Considering this issue along with selection of most abundant phenolic acids present in the two extracts, the probable mechanism of bioreduction has been depicted in Fig. 9 and Fig. 10.

CONCLUSION

The results of this research study demonstrated the most probable mechanisms for green synthesis of CuO-Cr_2O_3-NiO nanocomposites and Cu-Cr-Ni-O nanoalloys using the reducing ability of *E. campestre* and *F. subpinnata* leaf extracts. Crystallite size of the synthesized NCs was significantly influenced by the type of reducing agents (*E. campestre* and *F. subpinnata* leaf extracts), which could be encouraging from the perspective of size-controlled NP synthesis. Probes into mechanistic aspects of synthesis using total phenolics/total flavonoids, FTIR, and HPLC studies led to specification of the most abundant phenolic acids in the two plant extracts as bioreducing agents and aliphatic, aldehyde amine, and nitrile groups as capping/stabilizing ligands. Dual behavior of the two plant extracts toward reducing the metal ions, which led to different structure of the nanomaterials (nanocomposites and nanoalloys), may be important regarding application fields of the products.

ACKNOWLEDGEMENTS

We gratefully acknowledge the Iranian nano Council, green technology laboratory of the university of Tehran, and chemical engineering research laboratory of the University of Mohaghegh Ardabili for the support of this work.

REFERENCES

1. Z. Vaseghi, A. Nematollahzadeh and O. Tavakoli, *Rev. Chem. Eng.*, **34**, 529 (2018).
2. N. Patra, A. C. Taviti, A. Sahoo, A. Pal, T. K. Beuria, A. Behera and S. Patra, *RSC Adv.*, **7**, 35111 (2017).
3. S. D. Lankiang, S. Baranton and C. Coutanceau, *Electrochim. Acta*, **242**, 287 (2017).
4. Z. Gu, H. Xu, D. Bin, B. Yan, S. Li, Z. Xiong, K. Zhang and Y. Du, *Colloids Surf., A*, **529**, 651 (2017).
5. Y. Cao, M. S. Denny Jr., J. V. Caspar, W. E. Farneth, Q. Guo, A. S.

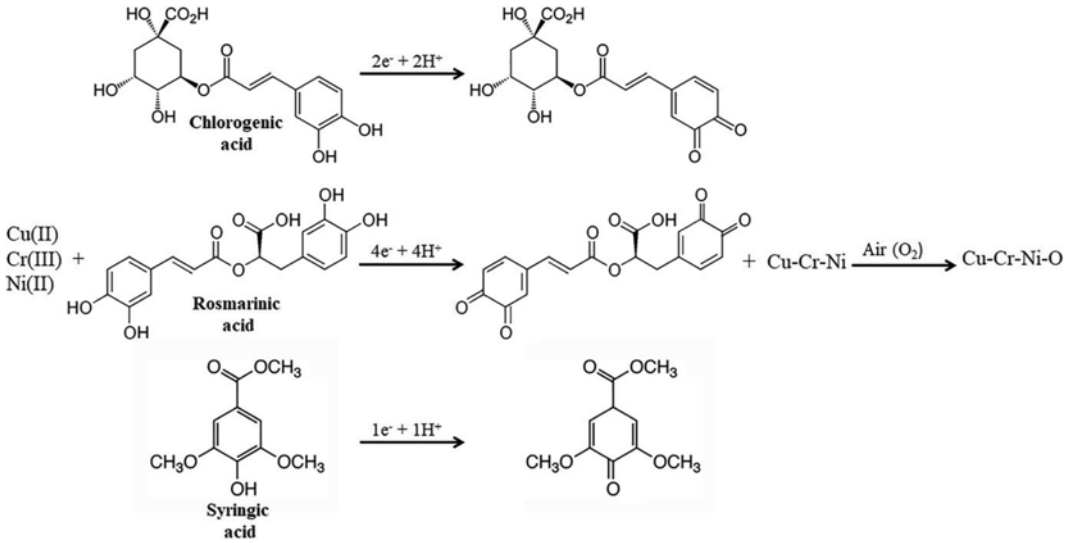

Fig. 10. Probable bioreduction mechanism for the synthesis of Cu-Cr-Ni-O nanoalloys using the phytochemicals in *F. subpinnata* leaf extract.

Ionkin, L. K. Johnson, M. Lu, I. Malajovich and D. Radu, *J. Am. Chem. Soc.*, **134**, 15644 (2012).
6. M. Moran, N. Rosell, G. Ruano, M. Busquets and M. Vinardell, *Colloids Surf., B*, **134**, 156 (2015).
7. J. Gu, X. Chen, H. Xin, X. Fang and X. Sha, *Int. J Pharm.*, **461**, 559 (2014).
8. S.-N. He, Y.-L. Li, J.-J. Yan, W. Zhang, Y.-Z. Du, H.-Y. Yu, F.-Q. Hu and H. Yuan, *Int. J. Nanomed.*, **8**, 2859 (2013).
9. F. Shaikh, L. Chikhale, I. Mulla and S. Suryavanshi, *Powder Technol.*, **326**, 479 (2018).
10. P. Elavarthi, A. A. Kumar, G. Murali, D. A. Reddy and K. Gunasekhar, *J. Alloys Compd.*, **656**, 510 (2016).
11. W. Weihua, T. Xuelin, C. Kai and C. Gengyu, *Colloids Surf., A*, **273**, 35 (2006).
12. M.-L. Wu, D.-H. Chen and T.-C. Huang, *Langmuir*, **17**, 3877 (2001).
13. K. Rawat and P. Shishodia, *Adv. Powder Technol.*, **28**, 611 (2017).
14. Y. Xia, B. Sun, Y. Wei, B. Tao and Y. Zhao, *J. Alloys Compd.*, **705**, 58 (2017).
15. M. P. Gashti, M. Burgener, M. Stir and J. Hulliger, *J. Colloid Interface Sci.*, **431**, 149 (2014).
16. M. Parvinzadeh Gashti, M. Helali and S. Karimi, *Int. J. Appl. Ceram. Technol.*, **13**, 1069 (2016).
17. M. P. Gashti, M. Stir and J. Hulliger, *New J. Chem.*, **40**, 5495 (2016).
18. M. P. Gashti and A. Shokri, *J. Aust. Ceram. Soc.*, **54**, 601 (2018).
19. Y. Dong, Z. Yang, Q. Sheng and J. Zheng, *Colloids Surf., A*, **538**, 371 (2018).
20. G. Wang, Z. Wen, L. Du, S. Li, S. Ji and J. Sun, *RSC Adv.*, **6**, 39728 (2016).
21. J. Liu, F. He, T. M. Gunn, D. Zhao and C. B. Roberts, *Langmuir*, **25**, 7116 (2009).
22. H. Duan, D. Wang and Y. Li, *Chem. Soc. Rev.*, **44**, 5778 (2015).
23. F. J. Osonga, I. Yazgan, V. Kariuki, D. Luther, A. Jimenez, P. Le and O. A. Sadik, *RSC Adv.*, **6**, 2302 (2016).
24. K. J. Rao and S. Paria, *ACS Appl. Mater. Interfaces*, **7**, 14018 (2015).
25. G. Zhan, J. Huang, M. Du, I. Abdul-Rauf, Y. Ma and Q. Li, *Mater. Lett.*, **65**, 2989 (2011).
26. B. Xia, F. He and L. Li, *Langmuir*, **29**, 4901 (2013).
27. Z. Vaseghi, A. Nematollahzadeh and O. Tavakoli, *J. Taiwan Inst. Chem. Eng.* (2018) HYPERLINK "https://doi.org/10.1016/j.jtice.2018.10.020"doi.org/10.1016/j.jtice.2018.10.020.
28. S. S. Shankar, A. Rai, A. Ahmad and M. Sastry, *J. Colloid Interface Sci.*, **275**, 496 (2004).
29. J. Kesharwani, K. Y. Yoon, J. Hwang and M. Rai, *J. Bionanosci.*, **3**, 39 (2009).
30. J. Kasthuri, K. Kathiravan and N. Rajendiran, *J. Nanoparticle Res.*, **11**, 1075 (2009).
31. Z. Vaseghi, O. Tavakoli and A. Nematollahzadeh, *J. Environ. Chem. Eng.*, **6**, 1898 (2018).
32. Z. Vaseghi, O. Tavakoli and A. Nematollahzadeh, *Int. Proc Chem. Biol. Environ. Eng.*, **101**, 62 (2017).
33. V. L. Singleton and J. A. Rossi, *Am. J. Enol. Vitic.*, **16**, 144 (1965).
34. J. Zhishen, T. Mengcheng and W. Jianming, *Food Chem.*, **64**, 555 (1999).
35. X. Fuku, N. Matinise, M. Masikini, K. Kasinathan and M. Maaza, *Mater. Res. Bull.*, **97**, 457 (2018).
36. S. A. Khan, F. Noreen, S. Kanwal, A. Iqbal and G. Hussain, *Mater. Sci. Eng.*, **82**, 46 (2018).
37. B. Sone, E. Manikandan, A. Gurib-Fakim and M. Maaza, *Green Chem. Lett. Rev.*, **9**, 85 (2016).
38. C. J. Pandian, R. Palanivel and S. Dhananasekaran, *Chinese J. Chem. Eng.*, **23**, 1307 (2015).
39. H. Chen, J. Wang, D. Huang, X. Chen, J. Zhu, D. Sun, J. Huang and Q. Li, *Mater. Lett.*, **122**, 166 (2014).
40. B. Ajitha, Y. A. K. Reddy, H.-J. Jeon and C. W. Ahn, *Adv. Powder Technol.*, **29**, 86 (2018).
41. T. Ataei-Germi and A. Nematollahzadeh, *J. Colloid Interface Sci.*, **470**, 172 (2016).
42. P. K. Singh, K. Bhardwaj, P. Dubey and A. Prabhune, *RSC Adv.*, **5**, 24513 (2015).
43. D. Dhamecha, S. Jalalpure and K. Jadhav, *J. Photochem. Photobiol.*, **154**, 108 (2016).
44. M. Fazlzadeh, K. Rahmani, A. Zarei, H. Abdoallahzadeh, F. Nasiri and R. Khosravi, *Adv. Powder Technol.*, **28**, 122 (2017).
45. C. Balalakshmi, K. Gopinath, M. Govindarajan, R. Lokesh, A. Arumugam, N. S. Alharbi, S. Kadaikunnan, J. M. Khaled and G. Benelli, *J. Photochem. Photobiol, B*, **173**, 598 (2017).
46. M. Kasithevar, M. Saravanan, P. Prakash, H. Kumar, M. Ovais, H. Barabadi and Z. K. Shinwari, *J. Interdiscip. Nanomed.*, **2**, 131 (2017).
47. M. Shahid, Z. H. Farooqi, R. Begum, K. Naseem, M. Ajmal and A. Irfan, *Korean J. Chem. Eng.*, **35**, 1099 (2018).
48. G. K. Deokar and A. G. Ingale, *RSC Adv.*, **6**, 74620 (2016).
49. M. Nasrollahzadeh and S. M. Sajadi, *J. Colloid Interface Sci.*, **462**, 243 (2016).
50. V. Ravichandran, S. Vasanthi, S. Shalini, S. A. A. Shah and R. Harish, *Mater. Lett.*, **180**, 264 (2016).
51. S. Conea, L. Vlase and I. Chirila, *Cellul. Chem. Technol.*, **50**, 473 (2016).
52. J. Hohmann, Z. Pall, G. Günther and I. Mathe, *Planta Medica*, **63**, 96 (1997).
53. S. M. Mohsen and A. S. Ammar, *Food Chem.*, **112**, 595 (2009).
54. T. J. I. Edison and M. Sethuraman, *Process Biochem.*, **47**, 1351 (2012).